The Use of TRMM Precipitation Radar Observations in Determining Ground Radar Calibration Biases

EMMANOUIL N. ANAGNOSTOU, CARLOS A. MORALES, AND TUFA DINKU

Department of Civil and Environmental Engineering, University of Connecticut, Storrs, Connecticut

(Manuscript received 4 April 2000, in final form 27 July 2000)

ABSTRACT

Since the successful launch of the Tropical Rainfall Measuring Mission (TRMM) satellite, measurements of a wide variety of precipitating systems have been obtained with unprecedented detail from the first space-based radar [precipitation radar (PR)]. In this research, a methodology is developed that matches coincident PR and ground-based volume scanning weather radar observations in a common earth parallel three-dimensional Cartesian grid. The data matching is performed in a way that minimizes uncertainties associated with the type of weather seen by the radars, grid resolution, and differences in radar sensitivities, sampling volumes, viewing angles, and radar frequencies. The authors present comparisons of reflectivity observations from the PR and several U.S. weather surveillance Doppler radars (WSR-88D) as well as research radars from the TRMM field campaigns in Kwajalein Atoll and the Large Biosphere Atmospheric (LBA) Experiment. Correlation values above 0.8 are determined between PR and ground radar matched data for levels above the zero isotherm. The reflectivity difference statistics derived from the matched data reveal radar systems with systematic differences ranging from +2 to −7 dB. The authors argue that the main candidate for systematic differences exceeding 1 to 1.5 dB is the ground radar system calibration bias. To verify this argument, the authors used PR comparisons against well-calibrated ground-based systems, which showed systematic differences consistently less than 1.5 dB. Temporal analysis of the PR versus ground radar systematic differences reveals radar sites with up to 4.5-dB bias changes within periods of two to six months. Similar evaluation of the PR systematic difference against stable ground radar systems shows bias fluctuations of less than 0.8 dB. It is also shown that bias adjustment derived from the methodology can have significant impact on the hydrologic applications of ground-based radar measurements. The proposed scheme can be a useful tool for the systematic monitoring of ground radar biases and the studying of its effect.

1. Introduction

Reliable quantitative information on the spatial and temporal distribution of rainfall is essential for hydrologic and climatic applications, which range from real-time flood forecasting to evaluation of global and regional atmospheric model simulations. Ground-based volume scanning weather radars can provide rainfall observations at spatiotemporal scales suitable for such applications. However, the complex radar measurement and the atmospheric characteristics associated with precipitation can contribute to significant uncertainties in the inferred rainfall. Several studies have addressed the problem of radar measurement effects, concentrating largely on the radar data quality (Moszkowicz et al. 1994; Austin 1987; Zawadzki 1984), reflectivity-to-rainfall (Z–R) transformation (Smith and Krajewski 1993; Scarchilli et al. 1990; Zawadzki 1982), and vertical reflectivity profile and beam geometry effects (Krajewski et al. 1996; Kitchen and Jackson 1993; Joss and Lee 1995; Rosenfeld et al. 1992).

An important error source, which can lead to significant systematic error in radar rainfall estimates, is the lack of accurate determination of the radar calibration constant (hereafter referred to as radar calibration bias). Smith et al. (1996) has shown that this error can cause significant radar-to-radar rainfall observation differences and should be quality controlled before applying any rainfall estimation algorithm. In a sensitivity study of the Z–R relationship, Ulbrich and Lee (1999) also underscored the need for absolute calibration of ground-based radars. For getting the exact radar constant, field tests using either metal spheres or active sources of radiation are required, which are labor-intensive processes and therefore quite infrequent. Currently, the problem of radar calibration bias has been addressed jointly with other systematic error sources through procedures that apply to radar–rain gauge rainfall accumulation comparisons (Anagnostou et al. 1998; Smith and Krajewski 1991). However, due to the large difference in the sampling geometry of the two sensors and

Corresponding author address: Emmanouil N. Anagnostou, Dept. of Civil and Environmental Engineering, University of Connecticut, 261 Glenbrook Road, U-37, Storrs, CT 06269-2037.
E-mail: manos@engr.uconn.edu

the high variability of the *Z–R* relationship, these comparisons are noisy and difficult to interpret (Anagnostou et al. 1999; Kitchen and Blackall 1992).

In this paper, we attempt to address the problem of radar calibration bias adjustment using observations from the first space-based radar [precipitation radar (PR)] aboard the recently launched Tropical Rainfall Measuring Mission (TRMM) satellite (Simpson et al. 1996). The PR, which has an attenuated frequency (13.8 GHz) and a nominal sensitivity threshold of about 17 dB*Z*, has been demonstrated by the National Space and Development Agency of Japan (NASDA) to be consistent with calibration stability within 0.8 dB (Kozu et al. 2000; Kawanishi et al. 1998, 2000). The goal of this research is to develop a methodology that uses PR observations to identify calibration biases in ground weather radar systems and assess its implications on radar-rainfall estimation accuracy. We base this investigation on the fact that PR and ground weather radar systems measure the same variable (i.e., reflectivity) and that PR is fairly consistent with respect to calibration accuracy. We use 6 months of coincident PR and ground radar data from 14 U.S. radar sites and TRMM field campaigns to demonstrate the proposed methodology. It is shown that PR observations can be used to systematically monitor the calibration coefficient of ground radar systems. Examples are provided, showing that adjusting the ground radar reflectivity measurements using bias coefficients derived from the proposed method can reduce the widely diverging rainfall accumulation differences between adjacent ground radars.

In the following section, we provide background information on the PR and the ground radar systems used in the study. A description of the methodology used to match PR and ground radar measurements is discussed in section 3. In section 4, we present the dataset. Qualitative comparisons are shown in section 5, while the reflectivity difference statistics for the selected radar sites are presented in section 6. The hydrological implications of the proposed methodology are discussed in section 7, while in section 8, we offer our conclusions and discussion for future research.

2. Background

The National Weather Service of the United States is using an extensive nationwide network of Weather Surveillance Radar-1988 Doppler (WSR-88D) units, also known as the NEXRAD system. The WSR-88D units are powerful 10-cm wavelength radars with approximately 1° beam width by 1-km range resolution and volume scan sampling frequency of ~6 min. Each volume scan consists of approximately 9 sweeps, with elevation angles ranging from 0.5° (base scan) to 19°. Heiss et al. (1990) and Crum et al. (1993) provide a detailed discussion on the WSR-88D characteristics. The NEXRAD system brings dramatic advancements to a wide range of hydrometeorological applications, and its information is readily visible to the earth science and engineering community. Nevertheless, its data have found less uses than expected due to limitations inherent in the use of radar to estimate precipitation. Although part of the problem has been ascribed to the uncertainties involved in the transformation from reflectivity to rainfall rate, it appears that inadequate calibration of the radar constant often contributes significant error (Hunter 1996; Smith et al. 1996; Anagnostou et al. 1998). Operationally, WSR-88D systems calibrate reflectivity for every volume scan using internally generated test signals, which are based on internal RF pulse injection into the receiver. It is expected that these calibration checks would maintain a calibration precision of 1 dB. Calibration drifts due to gradual degradation of the system performance (gain, loss, antenna, radome changes, etc.), which cannot be detected by the above internal calibration process, are the most likely cause of reflectivity differences observed at the same locations from adjacent WSR-88Ds (e.g., Smith et al. 1996; Ricks et al. 1995).

The TRMM field experiment at the Kwajeleign Atoll (KWAJEX) employed a network of two radars, namely a C-band Doppler and an S-band polarimetric (hereafter called KWAJEX S band) Doppler radar. The TRMM Large Biosphere Atmospheric (LBA) experiment also employed a network of two radars: National Aeronautics and Space Administration's (NASA's) C-band Doppler radar (hereafter caller LBA–TOGA) and National Center for Atmospheric Research's (NCAR's) S-band Doppler polarimetric radar (hereafter called LBA–SPOL). The KWAJEX S-band and LBA–SPOL systems sample with a 1° beam width and range gates of ~250 m (256 m for KWAJEX S band). The TOGA research radar has 1.656° beamwidth and range resolution of 250 m. In the event of full volume scans, the elevation sweeps of these radars extend above 20° elevation angles. A main objective of TRMM field experiments is to obtain reliable quantitative estimates of rainfall from the employed ground radars. This would require determination of the radars' absolute calibration. Subsequently, systematic differences between PR and field campaign radar reflectivity observations should be explained and adjusted before any attempt is made for estimating rainfall.

The precipitation radar onboard TRMM has a 13.8-GHz frequency (2.2-cm wavelength), an approximately 4.5-km spatial resolution at near nadir, and a 250-m vertical resolution. The radar has a nominal sensitivity of approximately 17 dB*Z*. The anticipated temporal sampling frequency over the United States is less than 11 h (Simpson et al. 1996). Performance characteristics and initial checkouts of the PR conducted by NASDA researchers (Kawanishi et al. 1998) confirmed that PR closely meets its design specifications (see Table 1). Furthermore, external calibration tests, using an active radar calibrator (ARC) located in Japan (Kumagai et al. 1995), have shown PR calibration stability within 0.8 dB (Kozu et al. 2000). Information on the PR system

TABLE 1. Results of PR initial checkout.

Items	Specification	Initial checkout
Peak power	>500 W	708 W
Antenna gain	47.4 dB	47.9 dB
Beamwidth		
Nadir	0.71° ± 0.02°	0.71°
Scan edge	0.74° ± 0.03°	0.74°
Sidelobe level	<−27 dB	−28 dB
Min det. level	<−110 dBm	110.2 dBm
Min det. rain rate	<0.7 mm h^{-1}	0.48 mm h^{-1}
Power consumption	<250 W	213 W

design, algorithms, and calibration procedures can be found in Kawanishi et al. (2000).

Routine monitoring of the PR calibration has been scheduled over the life of the instrument to continue testing its stability. Monitoring is based on the 1) ARC, which is testing the radar transponder, receiver, and beacon transmitter, and 2) rain-free ocean backscatter measurements within 10° incidence. After almost 2 yr of PR operations it is shown that 1) the correction factor determined from the ARC is about 0.6 dB, which is well within the bias error estimation, and 2) the ocean surface cross section at 10° incidence measured by the PR is within 0.2-dB agreement with previous measurements by airborne radars of the same frequency (Kozu et al. 2000). Finally, comparisons of mean monthly 1° surface cross sections derived from TOPEX altimeter and PR observations at near nadir have shown less than 0.5-dB differences (R. Meneghini 1999, personal communication). The above tests have indicated that PR is capable of providing reflectivity measurements with less than a 0.8-dB calibration error.

Finally, we note that since PR is a 2.2-cm wavelength radar, it is subject to more two-way path integrated attenuation than the 10-cm wavelength ground radar systems. We use attenuation-corrected PR reflectivities derived from a hybrid method that is based on the Hitschfeld–Bordan iterative scheme, which performs well at low attenuations, and the surface reference method for which the relative error decreases with increasing path attenuation (Iguchi and Meneghini 1994). Iguchi et al. (2000) offer description and evaluation of the hybrid method as it applies to TRMM data. One should also expect range-dependent sampling differences between PR and ground-based radars. Finally, we note that most of the ground radar sampling volume scans have gaps at higher elevation sweeps (e.g., for WSR-88Ds, it is 3.5°, 6°, 9°, 14°, etc.), which may introduce interpolation errors when compared to the high vertical resolution (250 m) PR samples. Other issues include the different viewing angles as well as signal frequency and sensitivity differences between space and ground radars. These issues are addressed in the following section, which describes our methodology.

3. Methodology

The purpose of the proposed methodology is the estimation of systematic errors in ground radar reflectivity measurements by comparing it to coincident PR observations. The method is based on a scheme that interpolates ground and space radar volume scans into a fixed grid and on a data selection that minimizes uncertainties associated with the issues described above. The interpolation scheme and data selection are described next.

Instantaneous PR and ground radar reflectivity volume scans that are within a time lag at a maximum of 3 min are projected into a common earth parallel three-dimensional Cartesian grid (hereafter called 3D-box) with 5 × 5 km horizontal and 2 km vertical resolution. The 3D-box pixel dimensions are selected to be consistent with both the ground radar's low vertical resolution (~2 km at 100-km range for 1° beamwidth) and the PR's field-of-view resolution (~4.5 × 4.5 km). The 3D-box is centered at each ground radar site with a horizontal extent of ±100 km and vertical levels ranging from a minimum of 2 km to a maximum of 10 km. Below 2 km, both PR and ground radar data may be contaminated by ground returns, while above 10 km, the gaps in upper elevation sweeps of ground radars may introduce significant interpolation errors. The actual lower and upper levels of each pixel within the 3D-box grid are variable and depend on the elevation of the zero isotherm and the highest elevation with detectable (>18 dBZ) PR reflectivity. Each ray of a PR swath is projected on the 3D-box using information about the spacecraft location and altitude (from a satellite navigation algorithm), the beam inclination, and a stereographic projection scheme. The projected PR reflectivity values ($mm^6\ m^{-3}$) are subsequently averaged in the vertical to produce the 3D-box pixel values.

The ground radar reflectivity volume scans are transformed from polar coordinates to the 3D-box through conversion tables. These tables indicate the radar polar samples and relative weights representing their volume fraction, which correspond to each 3D-box pixel. They are constructed using an algorithm that simulates the radar sampling process (Anagnostou and Krajewski 1997) accounting for beam propagation, refraction, and widening, according to a specified radar sampling geometry and mean refractive index profile (Battan 1973). Refractive index profiles are determined based on the nearest in time and space atmospheric sounding data or, in a more simplified form, using the four-thirds earth radius model of the refractive index profile (Doviac and Zrnic 1993). Since the radar sampling (elevation sweeps, azimuth, and range samples, etc.) may vary from scan to scan, radar volume scans are interpolated to a fixed polar grid before their conversion to the 3D-box. The fixed polar grid resolution is defined according to the radar sampling specifications, namely beam width, range averaging, and elevation angles. The interpolation of the variable polar radar samples to the

fixed polar grid is based on the square-inverse distance method. The fixed polar grid for the WSR-88D systems is defined at polar cells of 1° azimuth and 1-km range resolution as well as 1° elevation increments starting at 0.5° base scan. For the KWAJEX S-band, LBA–SPOL, and LBA–TOGA radars, the fixed polar grid range resolution is defined to 250 m due to the higher resolution of their data, while the azimuth and elevation angles are kept to 1°, with the exemption of TOGA radar, for which the azimuth fixed polar grid resolution is set to 1.66°.

Although the above matching scheme can minimize uncertainties associated with the sampling resolution differences of the two radars, additional steps are needed to make the PR–ground radar comparisons meaningful for the purpose of identification of calibration biases. The steps are 1) attenuation correction of the raw PR reflectivity profiles; 2) classification of precipitation systems to convective, stratiform, and mixed type; 3) determination of the bright band (mixed phased hydrometeors) level; and 4) definition of the lower and upper levels for each vertical column of the 3D-box. The method uses attenuation-corrected PR reflectivity values retrieved from the TRMM Science Data and Information System (TSDIS) 2A-25 algorithm (Simpson et al. 1996), documented in Iguchi and Meneghini (1994). The algorithm, which combines the iterative scheme of Hiltschfeld–Bordan with a surface reference method, has been shown using TRMM data that can offer great attenuation correction accuracy (Iguchi et al. 2000). The precipitation classification and bright band level determination are two products provided by the TSDIS 2A-23 algorithm, which is based on algorithms described in Iguchi et al. (2000). The lower level for each grid in the 3D-box is defined as the level of the first pixel above the bright band, while the upper level is the upper most pixel level where all PR samples that contribute to the pixel average exceed the 18-dB*Z* threshold. We eliminate sections of the 3D-box that are classified as mainly convective. This serves to reduce uncertainty due to the high subgrid precipitation variability associated with these systems and random effects due to changes of precipitation type. Furthermore, constraining the analysis above the bright band and to mainly stratiform systems eliminates uncertainties associated with attenuation correction errors. Finally, the viewing angle and signal frequency (non-Rayleigh effect) differences between PR and ground radars are more minor issues when considering frozen phase hydrometeors (precipitating ice, snow, etc.) and reflectivity values of less than 35 dB*Z*.

The final step of our methodology is the evaluation of the systematic difference between the PR and ground radar data. Two methods are applied to the selected 3D-box matched reflectivity values. The first method is based on the sample statistics of the reflectivity differences (in dB), namely, the mean (B_{smp}) and standard deviation (σ_{smp}):

$$B_{\text{smp}} = \frac{1}{n}\sum_{n}(Z_{\text{GR}} - Z_{\text{PR}}), \tag{1}$$

$$\sigma^2_{\text{smp}} = \frac{1}{n}\sum_{n}[(Z_{\text{GR}} - Z_{\text{PR}})^2] - B^2_{\text{smp}}, \tag{2}$$

where Z_{GR} and Z_{PR} are the selected 3D-box matched reflectivity values (in dB*Z*) of the ground radar and PR, respectively, and n is the sample size. The standard deviation of the difference is used to derive the confidence interval (L) for the estimated mean difference (B_{smp}):

$$L = \pm t_a \frac{\sigma_{\text{smp}}}{\sqrt{n}}, \tag{3}$$

where t_a is the ath quantile point of the t distribution with n degrees of freedom.

The second method evaluates the bias coefficient (B_{pdf}) that minimizes an objective function (f) that measures the square difference between the frequency distributions of the two matched radar data. The objective function is defined as

$$f(B_{\text{pdf}}) = \frac{1}{n_1}\sum_{i=1}^{n_1}[(f_{\text{GR}}(Z_i + B_{\text{pdf}}) - f_{\text{PR}}(Z_i))Z_i]^2, \tag{4}$$

where f_{GR} and f_{PR} are the jumps of ground radar and PR reflectivity step cumulative density functions at discrete values Z_i, respectively, and n_1 is the number of these discrete steps. It is noted that the estimation of B_{pdf} with this method is subject to significant uncertainty for small sample sizes (<100).

4. Data

A procedure is used that is based on TRMM satellite navigation information and TRMM rainfall products and identifies overpasses with significant coincident precipitation coverage within a 100-km radar radius of a specified ground radar site. In this study, we concentrated on 14 U.S. WSR-88D sites and 3 experimental radars from the TRMM field campaigns in Kwajeleign atoll and LBA. For the WSR-88D sites, we considered matched cases with common precipitation coverage larger than 20% for the period December 1997 to September 1998. For the KWAJEX S-band radar, we used eight storm cases with significant common precipitation coverage from the period of August to December 1999, while for the LBA TOGA and SPOL radars, we identified six and four, respectively, coincident cases from the period of January–February 1999. For each selected case, we produced corresponding PR and ground radar 3D-box reflectivity fields according to the methodology described in section 3. The selected radar sites are shown in Fig. 1. A summary of the matched PR and ground-based radar data statistics is shown in Table 2. Figure 2 shows histograms of the WSR-88D 3D-box reflectivity values selected for use in the radar-difference analysis (solid line) and of the reflectivities classified as

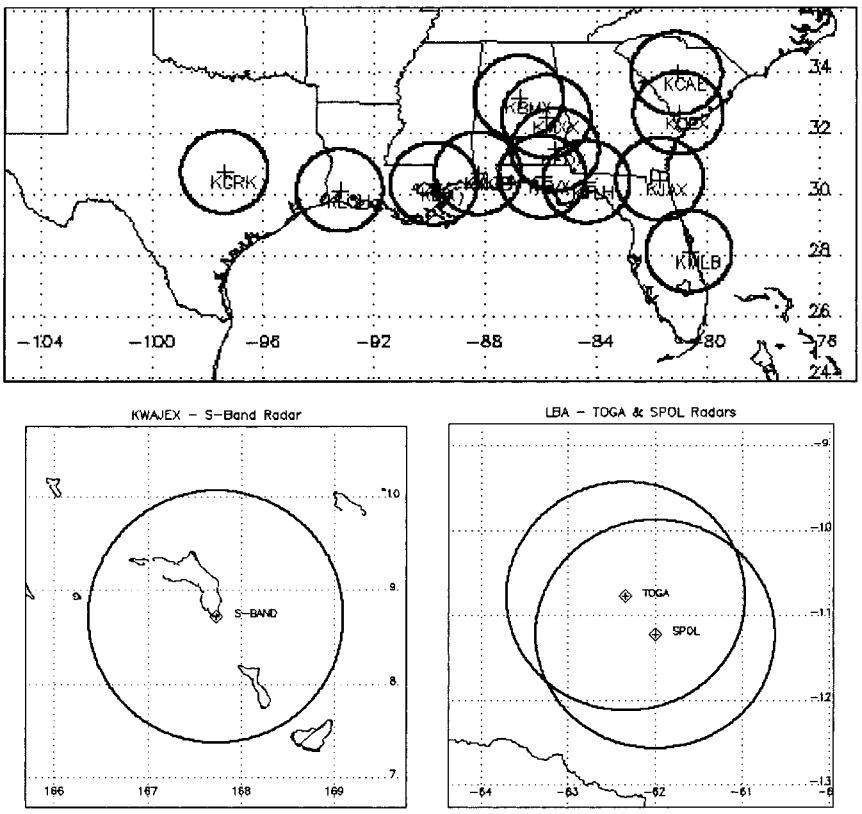

FIG. 1. The selected WSR-88D sites (upper panel), the KWAJEX S-band radar site (lower right panel), and the SPOL and TOGA sites in LBA (lower right panel) with circles corresponding to 150-km range.

inappropriate by our screening process and excluded by the statistical analysis (dashed line).

5. Qualitative comparison between PR and ground radars

In this section, we present matched cases of PR and ground-radar reflectivity data. This presentation shows the degree of agreement between the two radar reflectivity spatial patterns and relative magnitudes. In this analysis, the 3D-box is modified to adjust to each radar sampling resolution. Namely, it has vertical resolution of 250 m for the PR data and 1 km for the ground radar data. The horizontal resolution is kept to 5 × 5 km for both PR and ground radars. We note that these 3D-box dimensions are not used in the evaluation of the difference statistics, which are based on matched data derived from the methodology described in section 3.

Figure 3 shows an example of horizontal reflectivity distributions (at 3-km level, CAPPI) and reflectivity cross-section profiles of the PR and KWAJEX S-band radar for a case (30 October 1999) with significant precipitation coverage in the overlapping area of the two radars. The figure has six panels. The upper three panels show the 3-km CAPPI and two cross-sections of the PR attenuation corrected data (2A-25). The lower three panels show the same plots but for the coincident KWAJEX S-band data. The radar circles shown in the figure have a 150-km radius. One can note that although the patterns and positioning of the systems are the same, there is significant difference in the relative magnitude of their

TABLE 2. Summary of the processed matched PR and ground-based radar data. The columns reading from left to right are the ground radar sites, number of matched cases, number of 3D-box pixels used in the statistics, and correlation.

Sites	Cases	Pixels	Corr.
Fort Hood, TX (KGRK)	1	557	0.97
Lake Charles, LA (KLCH)	3	1808	0.94
Mobile, AL (KMOB)	5	3812	0.95
New Orleans, LA (KLIX)	3	1316	0.90
Birmingham, AL (KBMX)	6	3665	0.93
Maxwell AFB, AL (KMXX)	1	300	0.80
Jacksonville, FL (KJAX)	2	919	0.90
Tallahassee, FL (KTLH)	4	3244	0.93
Eglin AFB, FL (KEVX)	2	930	0.90
Fort Rucker, AL (KEOX)	5	1649	0.90
Charleston, VA (KCLX)	3	1460	0.89
Columbia, VA (KCAE)	9	7569	0.92
Melbourne, FL (KMLB)	4	820	0.85
TRMM Field Campaign, KWAJEX S-Band	8	1321	0.82
TRMM Field Campaign, LBA TOGA	6	1245	0.82
TRMM Field Campaign, LBA SPOL	4	380	0.88

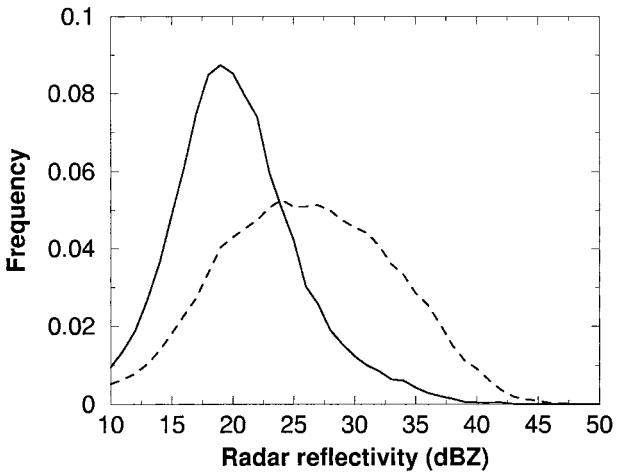

FIG. 2. Histograms of the WSR-88D reflectivity values used in the difference statistics (solid line) and of the values excluded (dashed line) as result of the screening criteria described in our methodology.

corresponding values. The cross-correlation between PR and KWAJEX S-band is 0.86 for zero space-lag and drops rapidly below 0.7 for lags greater than 1. One can also note the higher sensitivity of the SPOL with respect to the PR, which does not see reflectivity values lower than 17 dBZ. This issue is addressed in evaluating the difference statistics by excluding these PR pixels from the analysis, as described in section 3.

Figure 4 shows similar plots of 3-km CAPPIs and reflectivity cross-section profiles for a matched case (21 May 1998) where PR and two WSR-88Ds observe the precipitation system simultaneously. The two WSR-88D systems are the Mobile, KMOB, and New Orleans, KLIX. The upper, middle, and lower two panels of Fig. 4 show the 3-km CAPPI and cross-section plots for KMOB, PR attenuation corrected (2A-25), and KLIX radar reflectivity observations, respectively. From this figure, one can note significant reflectivity differences between the two adjacent ground radar sites (i.e., KMOB vs KLIX). Visual comparison of these ground radar reflectivity fields (upper and lower panels) against the corresponding PR observations (middle panel) shows that the KMOB radar has systematically lower values than the PR and corresponding KLIX radar values, which are in much better quantitative agreement. The above figures demonstrate the potential of using PR observations in identifying ground radar systems with calibration problems (the KMOB and KWAJEX S-band radars in the above example). This is further elaborated in the following section by presenting quantitative com-

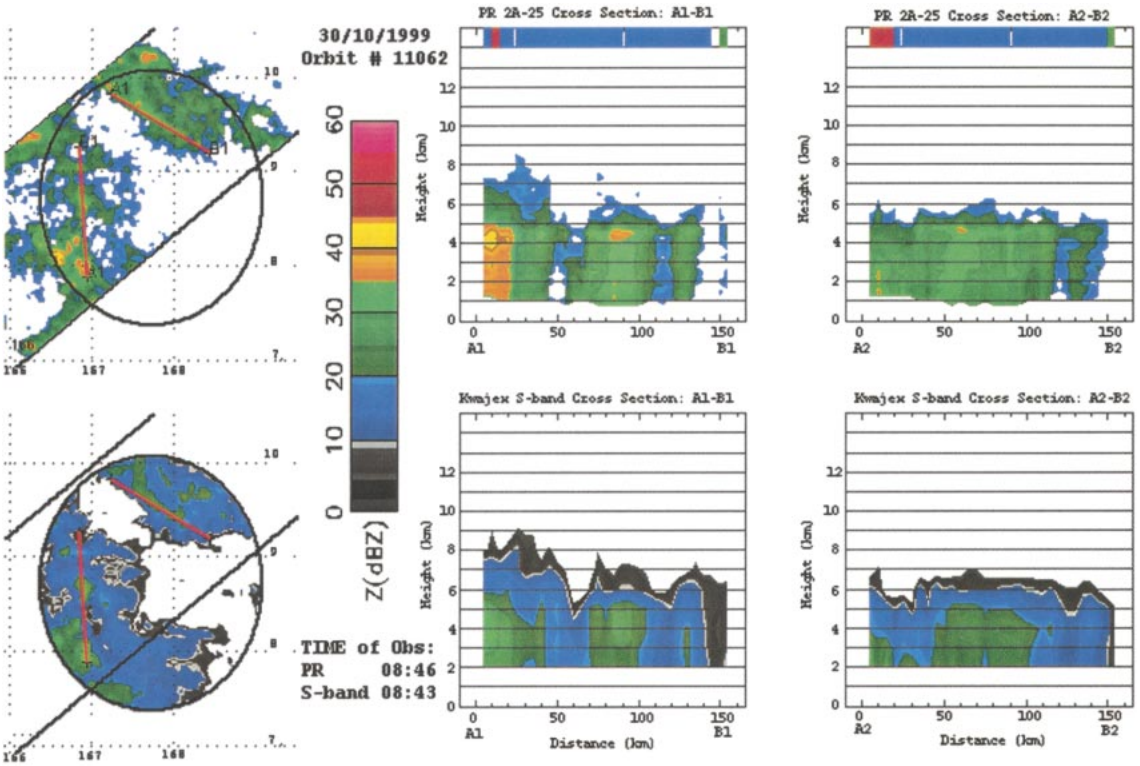

FIG. 3. Comparison of reflectivity fields at 3-km CAPPI and two vertical cross sections from the attenuation corrected PR (2A-25) and the KWAJEX S-band for the 30 Oct 1999 matched case. The color bar on the top of cross sections shows the precipitation type derived from TRMM 2A-23 algorithm (red: convective; green: stratiform; and blue: mixed type). The PR and ground radar vertical resolutions are 0.25 and 1 km, accordingly.

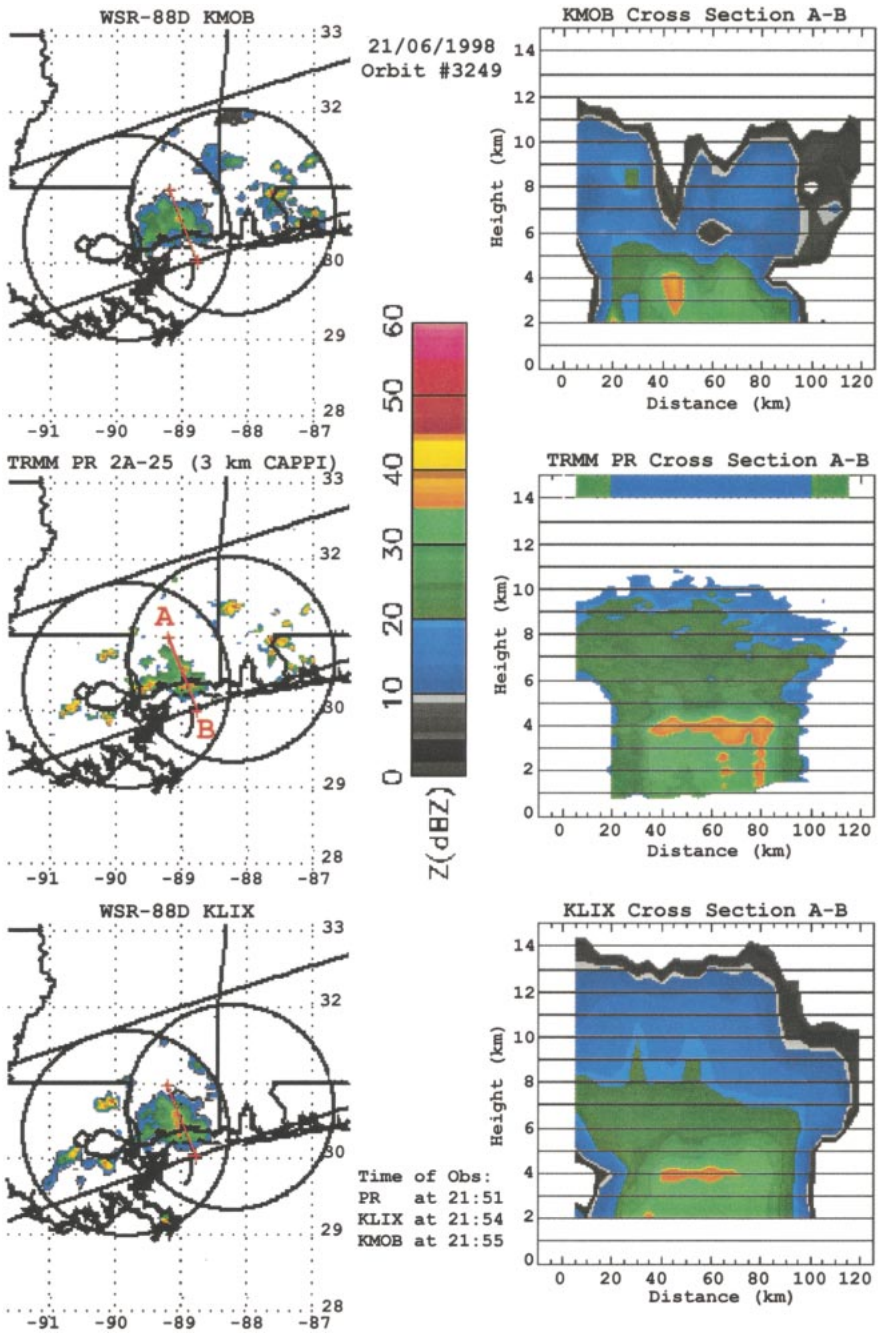

FIG. 4. Comparison of reflectivity fields at 3-km CAPPI and a vertical cross section from the attenuation corrected PR and two WSR-88Ds (KMOB and KLIX) for the 21 Jun 1998 matched case. The color bar on the top of cross sections and radar data resolutions are as in Fig. 3.

parisons of the matched PR and ground radar data. Note the higher vertical resolution of PR data compared to the WSR-88D systems. The bright band is resolved in greater detail by the PR while the WSR-88Ds smooth out significantly. The problem of differences in sampling resolutions is addressed by first constraining the quantitative analysis at ground radar ranges up to 100 km and then using a common 3D-box with pixel dimensions that correspond to the sampling resolution of both sensors (i.e., $5 \times 5 \times 2$ km). Furthermore, the quantitative analysis uses data samples from 3D-box levels that are above the bright band and below the level that PR reaches its lowest threshold. In the example of Fig. 4, these levels would have been from 5 to 9 km.

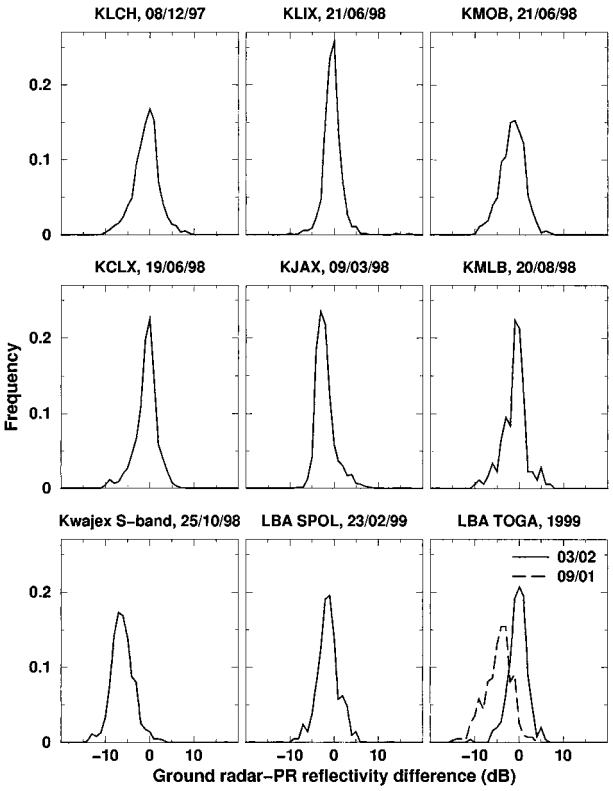

FIG. 5. Histograms of ground radar–PR reflectivity differences (dB) for selected matched cases. The time lags between PR and ground radar observations for these cases are less than 1.5 min.

6. Statistical analysis

This section presents quantitative comparisons between PR and ground radar observations for the data periods and sites described in section 4. The data used in this analysis are the $5 \times 5 \times 2$ km 3D-box interpolated reflectivity values selected according to the procedure described in our methodology. We first present (see Fig. 5) ground radar–PR reflectivity difference (in dB) histograms for selected WSR-88D sites and the KWAJEX S-band, LBA–SPOL, and LBA–TOGA radars. A first observation extracted from Fig. 5 is that the reflectivity difference histograms have shapes close to normal distribution, with standard deviations ranging between 1.5 and 2.5 dB. This variability is attributed to random effects associated with the hydrometeors size distribution variability, residual attenuation correction errors, incomplete knowledge of the ground radar beam propagation, ground radar interpolation errors due to gaps in their upper elevation sweeps (up to 4°), and temporal lags (up to 3 min) between PR and ground radar measurements. Nevertheless, one can clearly distinguish the ground radar sites, which have significant systematic differences against the PR observations. The WSR-88D sites with the most obvious systematic differences are the KMOB (−2.7 dB) and KJAX (−2.5 dB), while the KWAJEX S-band radar has the most significant difference (−7 dB) against the PR. For the LBA–TOGA radar, we show two histograms corresponding to coincident cases before and after 30 January 1999. This demonstrates a calibration shift in TOGA radar, which is further analyzed below in this section.

In the following, we examine the dependence of the PR ground radar reflectivity differences on the reflectivity magnitude itself. Figure 6 shows scatter plots of the mean reflectivity versus reflectivity difference values of the matched 3D-box PR and ground radar data. It is apparent from Fig. 6 that there is no obvious dependence of the reflectivity difference on the reflectivity magnitude. The reflectivity values in this plot are less than 40 dBZ, which is a result of the constraints posed by our methodology in the selection of the matched 3D-box data. Furthermore, classification of the reflectivity differences with respect to the level above the bright band has shown no obvious dependence. These two observations support the use of a fixed multiplicative coefficient, which is evaluated from the matched dataset according to Eqs. (1) or (4) and applied uniformly to the whole ground radar measurements.

A second issue associated with the ground radar bias is its temporal variability, which is due to gradual degradations of the system performance (gain, loss, antenna, etc.) or changes in the system characteristics (e.g., painting radome, changing electronics, human factor). We demonstrate significant (see Figs. 7a,b) time variations of the ground-based radar bias (in dB) estimated from Eq. (1) for several radar sites used in this study. Figure 7a shows bias time series for some of the WSR-88D sites, while Fig. 7b shows bias time series for the KMLB WSR-88D and three TRMM field campaign radars. The horizontal axis of the panels of these figure shows the dates of the matched datasets used in the bias estimates. The vertical bars plotted for each bias estimate represent its 95% confidence intervals evaluated using Eq. (3). These bounds represent the range of uncertainty of the estimated ground radar bias, which is a function of the sample size used in the estimation and the reflectivity difference variance. It is noted that any temporal variation of the bias may be considered significant if it exceeds the range of the confidence bounds of its estimate. The two horizontal lines in Fig. 7b correspond to the overall bias estimates derived from our two methods, namely, the sample mean (solid line) and the probability distribution matching (dashed line). For those WSR-88D sites (KCAE, KBMX, KMOB) that the matched datasets are at close time lags (2 h apart), we show that the bias fluctuations are either insignificant or slightly exceeding the confidence bounds of the bias estimates. It should be noted that the ground radar data used in this analysis have been corrected by the internal calibration applied by the radar systems. For some WSR-88D sites (e.g., KBMX, KCLX, KLCH), Fig. 7a shows long temporal stretches with the same calibration bias interrupted by an abrupt change to a different bias value. For the KCAE site, for example, before 19 Jan-

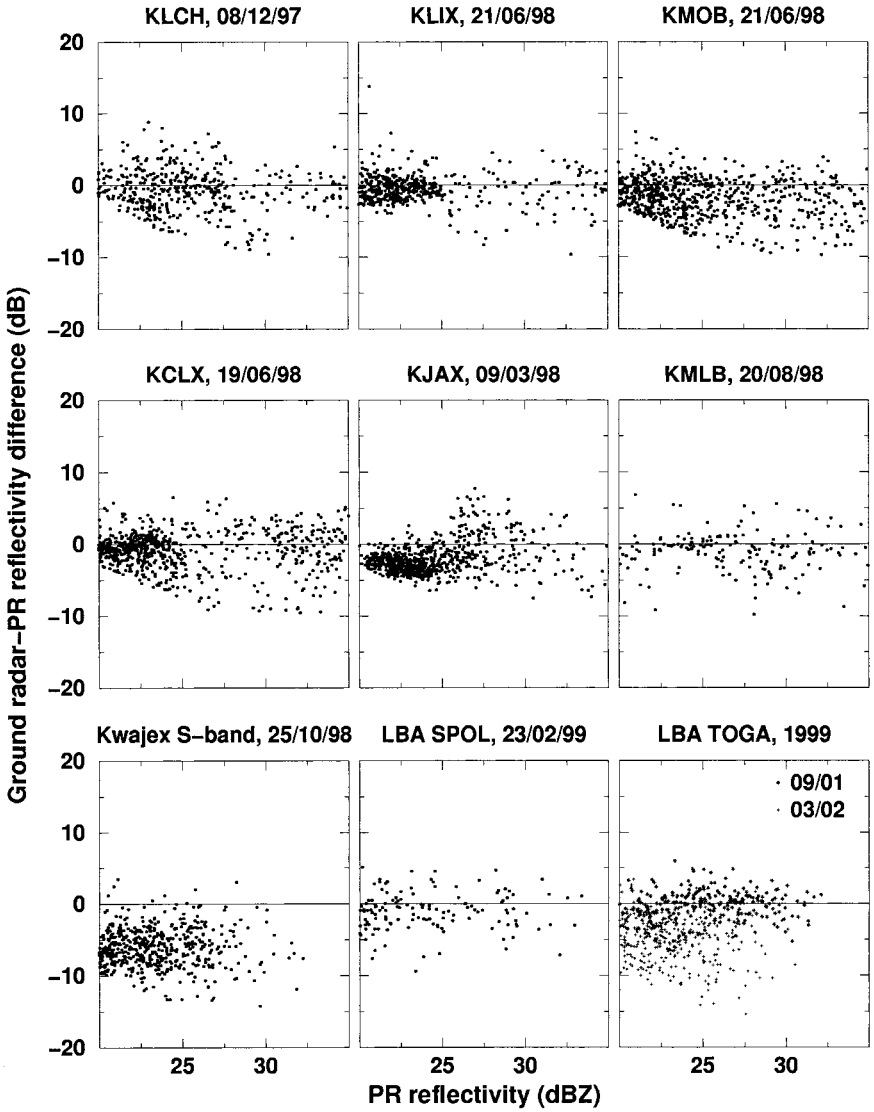

FIG. 6. Scatterplots of reflectivity differences vs the corresponding PR reflectivity values for the cases presented in Fig. 5.

uary 1998, its radar bias value was fluctuating around +1 dB, and progressively, (within a period of 8 months), the calibration bias changed to about −2 dB.

Similar observations are made for the LBA–TOGA radar (see the upper panel of Fig. 7b) calibration bias, where it is shown that the systematic difference with the PR changes from about −0.8 dB for the period ending 25 January to approximately −4.5 dB for the period after 1 February 1999. The variability of the systematic differences within each of the two distinct periods is ±0.8 dB, which is within the calibration accuracy of the PR. To verify the validity of this estimate, we used corresponding PR versus LBA–SPOL comparisons (see the second panel of Fig. 7b) from the same period. It is noted that the SPOL system is a state-of-the-art research instrument with consistent performance demonstrated in numerous past field experiments. As it is shown in Fig. 7b (second panel), the estimated systematic differences between PR and SPOL are consistently around −1.3 dB throughout the whole LBA period, with a random variation of less than 0.5 dB. Subsequently, the ~4.5-dB jump in the PR–TOGA comparisons may not be attributed to the methodology or the PR instrument, but mainly on a likely change of TOGA's calibration. We present further evidence of the validity of this estimate using rain gauge data. For this exercise, we used a *Z–R* relationship with fixed exponent coefficient (1.8) and an intercept parameter adjusted for the overall bias. Figure 8 shows the adjusted and unadjusted radar-to-gauge (R–G) biases for the periods before and after 27 January. The R–G bias change between the two periods is about 45% for the unadjusted

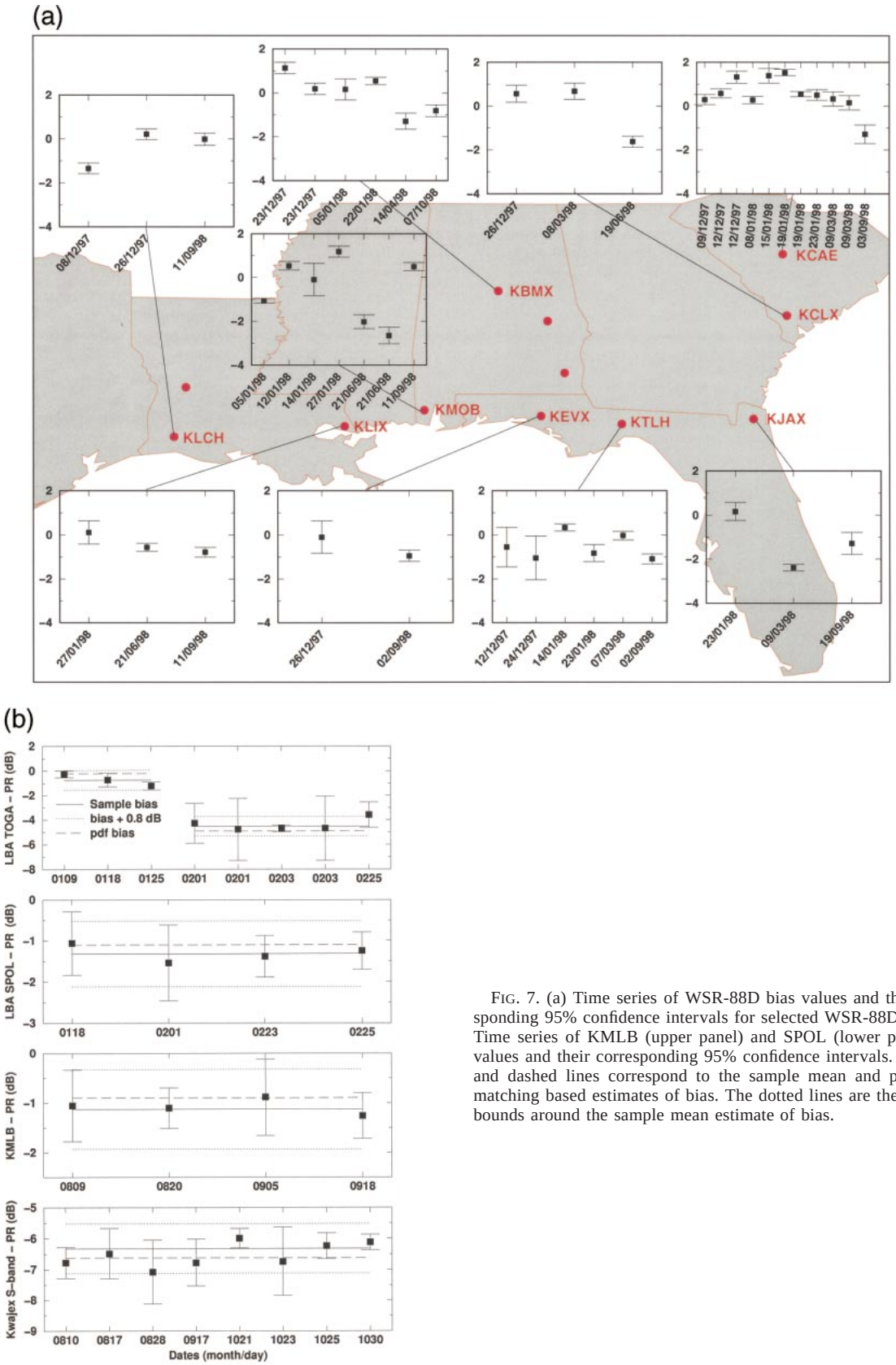

FIG. 7. (a) Time series of WSR-88D bias values and their corresponding 95% confidence intervals for selected WSR-88D sites. (b) Time series of KMLB (upper panel) and SPOL (lower panel) bias values and their corresponding 95% confidence intervals. The solid and dashed lines correspond to the sample mean and probability matching based estimates of bias. The dotted lines are the ±0.8 dB bounds around the sample mean estimate of bias.

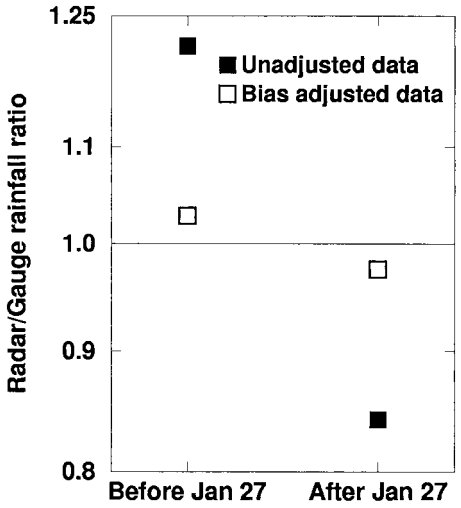

FIG. 8. Ratios of total gauge to total TOGA estimated rainfall for time periods before and after 27 Jan 1999. The open and solid boxes correspond to bias-adjusted and unadjusted reflectivity values.

TOGA data, which is consistent with the bias change shown in Fig. 7b (upper panel). After applying the suggestive by the PR bias correction (−4.5 dB), in the second period, the change in the R–G value between the two periods drops to 4%.

The lower two panels of Fig. 7b show time series of PR systematic differences against ground radar systems that are considered to be stable. The radars are the KMLB WSR-88D in Melbourne, Florida, with data provided by the Texas Florida Underflights Field Experiment (TEFLUB-B) for the period of 5 August to 27 September 1998 and the KWAJEX S-band radar described in section 4. Both radars are well-monitored systems, with relative calibration stability maintained by frequent internal calibration tests. It is shown that the temporal fluctuation of the bias for both radars is less than 0.5 dB, which is well within the calibration accuracy of the PR. Furthermore, is shown that the bias estimates derived using Eqs. (1) and (3) are similar (within 0.3 dB), which statistically verifies the observation that the reflectivity differences (in dB) are Gaussian random variables.

7. Hydrologic implications

The implication of the bias estimates derived based on the instantaneous PR and WSR-88D matched data is investigated on the basis of radar rainfall estimation accuracy. As we mentioned earlier, the WSR-88D systems provide detailed rainfall information that is readily available to the earth science community. However, these data have found limited uses by the operational hydrologic community due to limitations associated with inadequate calibration of the radar units, which lead to widely diverging rainfall estimates between adjacent radars. In a report by Ricks et al. (1995), it was concluded that these radar-to-radar differences introduce a situation that must be mitigated to provide more accurate hydrologic forecasts. In their report, an example was shown where hydrologic prediction of a widespread event, equidistant from two adjacent WSR-88Ds (KMOB and KLIX), varied from moderate to none river flooding by using the rainfall estimates from the two WSR-88D measurements.

Four years later, we identify a similar situation with the same two WSR-88Ds located almost equidistant from a precipitation system, but now they have the PR providing an independent view of the rainy area. Figure 3 described in section 3 shows that KMOB radar measures systematically less reflectivity values against the PR and KLIX radar. The systematic difference of KMOB and KLIX reflectivity values against the PR is −2.8 and −0.4 dB, respectively. This results in a radar-to-radar bias of 2.4 dB. The significance of this radar-to-radar bias on rainfall estimation is demonstrated in Fig. 9. Figure 9 shows—within the overlapping area of the two WSR-88Ds—plots of the difference between the storm total rainfall accumulation derived by the two radar measurements, raw (right panel) and adjusted (left panel) for the bias determined by the instantaneous matched dataset. The accumulation period is approximately 3 h, and the rainfall estimation was based on the WSR-88D rainfall algorithm (Anagnostou and Krajewski 1998). The bias adjustment significantly reduced the radar-to-radar differences, while in some parts of the rain area, the reduction is from above 15 to less than 5 mm (∼70%). This reduction in radar-to-radar rainfall bias is expected to have significant impact on hydrologic forecasting, as a recent study by Borga et al. (2000) has demonstrated that nonlinearities in rainfall–runoff transformation can magnify rainfall biases in hydrologic simulation.

8. Conclusions

A methodology has been developed that matches satellite and ground radar measurements in a common earth parallel three-dimensional grid (named 3D-box) with 5-km horizontal and 2-km vertical resolution. The methodology uses satellite navigation information, a radar sampling geometry model accounting for ray propagation under vertically stratified refractive index, and polar-stereographic projection to interpolate (i.e., latitude, longitude, height) satellite and ground radar data in a fixed 3D Cartesian grid (3D-box). The methodology provides an attractive framework for routine monitoring of ground radar system calibration biases over the globe, using as reference the stable Tropical Rainfall Measuring Mission (TRMM) satellite radar (PR) measurements.

The methodology was applied on coincident measurements from several WSR-88D units in the United States and three ground radars used in TRMM field campaigns. We demonstrated good matching between the ground radar and PR reflectivity patterns, with cor-

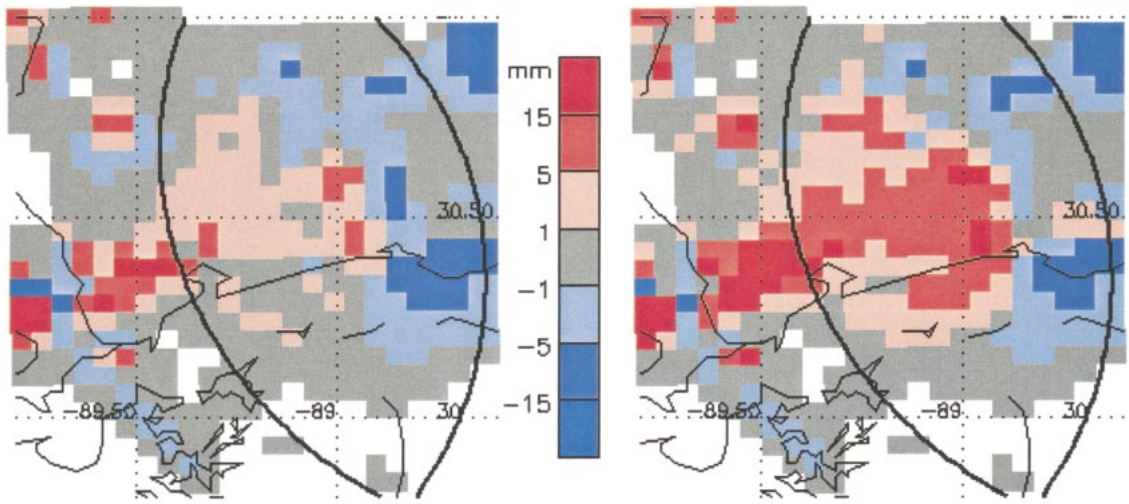

FIG. 9. Storm total rainfall accumulation differences between two WSR-88D radars (KMOB and KLIX). The left panel corresponds to reflectivity values corrected using the bias-adjustment factor evaluated from the 21 Jun 1998 matched case, while the right panel corresponds to unadjusted radar data. The solid lines represent the 150-km radar ranges.

relations at levels above the bright band varying from 0.8 to 0.95. Evaluation of the difference statistics revealed ground radar sites with significant bias (from +2 to −7 dB), which is attributed mainly to radar calibration. It was concluded that the bias has no obvious dependence on the reflectivity magnitude and on altitude. The temporal fluctuation of the radar bias was not significant at the storm scale, but at longer scales, we did show cases with significant variation (up to 4.5 dB). Assessment of the bias fluctuations using comparisons between PR and stable ground radar systems as well as rain gauge rainfall accumulation data showed consistent bias estimates. Application of our method to two well-calibrated S-band radar systems, namely the SPOL radar used in LBA and the KMLB WSR-88D, showed systematic differences ranging from −1 to −1.5 dB, which are expectable values considering the calibration accuracy of the PR (~0.8 dB) and potential non-Rayleigh effects (~0.5 dB).

The hydrologic implication of adjusting for the bias identified by the proposed methodology was shown to be significant. An example was shown where by applying the bias adjustment, the storm total rainfall accumulation difference between two adjacent WSR-88Ds dropped by up to 70%.

We continue our efforts on several extensions of the presented work. We are expanding our current database, including several new cases from the U.S. WSR-88D sites as well as international sites (e.g., South American radar networks). The current compiled database may be viewed on the World Wide Web (http://www.engr.uconn.edu/~gracp). We are also working on the development of a simulation framework in an effort to understand the physical causes of the variability observed in the matched PR and ground-based radar data.

Acknowledgments. The investigators acknowledge and appreciate insightful discussions and support by Dr. Christian Kummerow of NASA Goddard Space Flight Center, Dr. Brad Ferrier of JCET/University of Maryland Baltimore County, and Dr. D.-J. Seo of the Office of Hydrology of National Weather Service. This research was funded by the Tropical Rainfall Measuring Mission of NASA (Grant #NAG5-7813). The WSR-88D data were provided free of charge by the National Climatic Data Center of NOAA. The KWAJEX S-band radar data were provided by Dr. Sandra Yuter of The University of Washington. The SPOL radar data were provided by Dr. Walt Petersen from Colorado State University. The NASA TOGA radar data were provided by NASA TRMM office. The PR data were available from DAAC of NASA Goddard Space Flight Center. Documentation of TRMM data was provided by TSDIS.

REFERENCES

Anagnostou, E. N., and W. F. Krajewski, 1997: Simulation of radar reflectivity fields: Algorithm formulation and evaluation. *Water Resour. Res.*, **33,** 1419–28.

——, and ——, 1998: Calibration of the WSR-88D Precipitation Processing Subsystem. *Wea. Forecasting,* **13,** 396–406.

——, ——, D.-J. Seo, and E. R. Johnson, 1998: Mean-field radar rainfall bias studies for NEXRAD. *ASCE J. Hydrol. Eng.*, **3,** 149–159.

——, ——, and J. Smith, 1999: Uncertainty quantification of mean-field radar-rainfall estimates. *J. Atmos. Oceanic Technol.*, **16,** 206–215.

Austin, P. M., 1987: Relation between measured radar reflectivity and surface rainfall. *Mon. Wea. Rev.,* **115,** 1053–1069.

Battan, L. J., 1973: *Radar Observation of the Atmosphere.* University of Chicago Press, 324 pp.

Borga, M., E. N. Anagnostou, and E. Frank, 2000: On the use of real-time radar rainfall estimates for flood simulation in mountainous basins. *J. Geophys. Res., Atmos.,* **105** (D2), 2269–2280.

Crum, T. D., R. L. Alberty, and D. W. Burgess, 1993: Recording, archiving, and using WSR-88D data. *Bull. Amer. Meteor. Soc.,* **74,** 645–653.

Doviak, R. J., and D. S. Zrnić, 1993: *Doppler Radar and Weather Observations.* 2d ed. Academic Press, 458 pp.

Heiss, W. H., D. L. McGrew, and D. Sirmans, 1990: Next Generation Weather Radar (WSR-88D). *Microwave J.,* **33,** 79–98.

Hunter, S. M., 1996: WSR-88D radar rainfall estimation: Capabilities, limitations and potential improvements. *Natl. Wea. Dig.,* **20,** 26–41.

Iguchi, T., and R. Meneghini, 1994: Intercomparison of single-frequency methods for retrieving a vertical rain profile from airborne or spaceborne radar data. *J. Atmos. Oceanic Technol.,* **11,** 1507–1516.

——, ——, J. Awaka, T. Kozu, and K. Okamoto, 2000: Rain profiling algorithm for TRMM precipitation radar data. *Remote Sens. Appl.: Earth Atmos. Oceans,* **25,** 973–976.

Joss, J., and R. Lee, 1995: The application of radar-gauge comparisons to operational precipitation profile corrections. *J. Appl. Meteor.,* **34,** 2612–2630.

Kawanishi, T., T. Kozu, R. Meneghini, J. Awaka, and K. Okamoto, 1998: Preliminary results of rain profiling with TRMM precipitation radar. *Proc. SPIE: Microwave Remote Sensing of the Atmosphere and Environment,* Beijing, China, International Society for Optical Engineering, 94–101.

——, and Coauthors, 2000: TRMM precipitation radar. *Remote Sens. Appl.: Earth Atmos. Oceans,* **25,** 969–972.

Kitchen, M., and R. M. Blackall, 1992: Representativeness errors in comparisons between radar and gauge measurements of rainfall. *J. Hydrol.,* **134,** 13–33.

——, and P. M. Jackson, 1993: Weather radar performance at long range. Simulated and observed. *J. Appl. Meteor.,* **32,** 975–985.

Kozu, T., and Coauthors, 2000: Development of precipitation radar onboard the Tropical Rainfall Measuring Mission (TRMM) satellite. *IEEE Trans. Geosci. Remote Sens.,* in press.

Krajewski, W. F., E. N. Anagnostou, and G. J. Ciach, 1996: Effects of the radar observation process on inferred rainfall statistics. *J. Geophys. Res., Atmos.,* **101** (D21), 26 493–26 502.

Kumagai, H., T. Kozu, M. Satake, H. Hanado, and K. Okamoto 1995: Development of an active radar calibrator for the TRMM precipitation radar. *IEEE Trans. Geosci. Remote Sens.,* **GE-33,** 1316–1318.

Moszkowicz, S., G. J. Ciach, and W. F. Krajewski, 1994: Statistical detection of anomalous propagation in radar reflectivity patterns. *J. Atmos. Oceanic Technol.,* **11,** 1026–1034.

Ricks, R., J. Graschel, and E. Jones, 1995: A Comparison of adjacent WSR-88D precipitation estimates along the Mississippi Gulf coast. NWS Tech. Attachment, Lower Mississippi River Forecast Center, Slidell, Louisiana, 12 pp.

Rosenfeld, D., D. Atlas, D. B. Wolff, and E. Amitai, 1992: Beamwidth effects on Z–R relations and area-integrated rainfall. *J. Appl. Meteor.,* **31,** 454–464.

Scarchilli, G., E. Gorgucci, T. A. Seliga, and K. Aydin, 1990: Effects of raindrop-size distribution variation within the radar scattering volume on radar observables. *J. Atmos. Oceanic Technol.,* **7,** 919–929.

Simpson, J., C. Kummerow, W.-K. Tao, and R. F. Adler, 1996: On the Tropical Rainfall Measuring Mission (TRMM). *Meteor. Atmos. Phys.,* **60,** 19–36.

Smith, J. A., and W. F. Krajewski, 1991: Estimation of the mean field bias of radar rainfall estimates. *J. Appl. Meteor.,* **30,** 397–412.

——, and ——, 1993: A modeling study of rainfall rate–reflectivity relationships. *Water Resour. Res.,* **29,** 2505–2514.

——, D.-J. Seo, M. L. Baeck, and M. D. Hudlow, 1996: An intercomparison study of NEXRAD precipitation estimates. *Water Resour. Res.,* **32,** 2035–2045.

Ulbrich, C. W., and L. G. Lee, 1999: Rainfall measurement error by WSR-88D radars due to variations in Z–R law parameters and the radar constant. *J. Atmos. Oceanic Technol.,* **16,** 1017–1024.

Zawadzki, I., 1982: The quantitative interpretation of weather radar measurements. *Atmos.–Ocean,* **20,** 158–180.

——, 1984: Factors affecting the precision of radar measurements of rain. *Proc. 22nd Radar Meteorology Conf.,* Zurich, Switzerland, Amer. Meteor. Soc., 251–256.